ELSEVIER

Journal of Alloys and Compounds 450 (2008) 426–431

Journal of ALLOYS AND COMPOUNDS

www.elsevier.com/locate/jallcom

Characterization and photocatalytic activity of Sm^{3+}-doped TiO_2 nanocrystalline prepared by low temperature combustion method

Qi Xiao [a,b,*], Zhichun Si [a], Zhiming Yu [b], Guanzhou Qiu [a]

[a] *School of Resources Processing and Bioengineering, Central South University, Changsha 410083, China*
[b] *School of Materials Science and Engineering, Central South University, Changsha 410083, China*

Received 2 August 2006; received in revised form 10 October 2006; accepted 29 October 2006
Available online 6 December 2006

Abstract

Sm^{3+}-doped TiO_2 nanocrystalline has been successfully prepared by low temperature combustion synthesis (LCS). Results showed that the samarium doping was found to be able to significantly inhibit the anatase–rutile phase transformation. Photocatalytic degradation experiments indicated that doping samarium ions in TiO_2 could enhance photocatalytic activity in photocatalytic degradation of methylene blue. The increase in photocatalytic activity is probably due to prevention of electron–hole recombination and the existence of a synergistic effect between anatase and rutile. The highest enhancement in photoreactivity was obtained at 0.5 mol% samarium ions doping, which may be in favor of the most efficient separation of the charge carriers. It has been found that the photocatalytic activity is drastically increased under the presence of a small amount of anatase phase (only 5.9% anatase) compared to pure rutile, and the sample calcined at 600 °C with 51.61% rutile shows the highest photocatalytic activity, which suggests the existence of a synergistic effect between anatase and rutile powders in the Sm^{3+}-doped TiO_2, which is similar to that of undoped TiO_2.

Keywords: Sm^{3+}-doped TiO_2 nanocrystalline; Low temperature combustion synthesis; Photocatalytic activity

1. Introduction

TiO_2-based photocatalytic oxidation techniques have received much attention to their potential application for complete mineralization of many toxic and non-biodegradable organics [1,2]. Unfortunately, the photocatalytic degradation efficiency on the surface of TiO_2 particles is still low, which is due to the fast recombination rate of photogenerated electron–hole pairs. In order to slow down the electron–hole pairs and enhance interfacial charge-transfer efficiency, several approaches have been proposed, including transition metals doping [3,4], coupled semiconductor systems [5,6], noble metals deposition [7] and rare earth ions doping [8–11]. Especially, doping with lanthanide ions with 4f electron configurations could significantly enhance the photocatalytic activity of TiO_2.

Various synthetic routes like sol–gel method [9], hydrothermal method [10], coprecipitation–peptization method [11] have been studied for rare earth doped TiO_2 nanocrystalline. Among these methods, the sol–gel process leads to the greatest possible homogeneous distribution of the dopant in the host matrix and high surface area TiO_2 particles. However, the drawback of the mentioned sol–gel route is the application of expensive raw material of tetra-isopropylorthotitanate and organic solvent, which was limited.

In this work, we focus on the synthesis of Sm^{3+}-doped TiO_2 powders by low temperature combustion synthesis (LCS)—a novel way and unique combination of the combustion process and the chemical gelation process. The LCS technique exploits the advantages of mixing of compositions at the level of atoms or molecules, synthesizing of ultrafine, homogeneous highly reactive powder, and simple preparation method. Moreover, nanosized powders can be crystallized directly without the need for post-heat treatment [12], which favors high photocatalytic activity of TiO_2 nanocrystalline. To my own knowledge, low temperature combustion method has seldom been used to prepare nanosized photocatalyst.

* Corresponding author at: School of Resources Processing and Bioengineering, Central South University, Changsha 410083, China. Tel.: +86 731 8830543; fax: +86 731 8879815.
E-mail address: xiaoqi88@mail.csu.edu.cn (Q. Xiao).

0925-8388/$ – see front matter © 2006 Elsevier B.V. All rights reserved.
doi:10.1016/j.jallcom.2006.10.137

In this study, high photocatalytic activity of Sm^{3+}-doped TiO_2 nanocrystalline was obtained via LCS method, which can be used as photocatalysts in aqueous solution. And effect of calcinations temperature and doping content of Sm^{3+} ions on photocatalytic activity of TiO_2 was discussed.

2. Experimental

2.1. Synthesis

Sm^{3+}-doped TiO_2 nanocrystalline was synthesized by low temperature combustion synthesis (LCS). The detailed process can be described as follows. The analytical grade titanium isopropoxide (Ti $(OC_2H_5)_4$)), Sm $(NO_3)_3$, $C_2H_6O_2$ (ethylene glycol, abbreviated as EG), $C_6H_8O_7$ (citric acid, abbreviated as CA), ammonia (25%) and nitride acid (65–68%) were used as raw materials. Appropriate amount of Ti $(OC_2H_5)_4$ and Sm $(NO_3)_3$ were added to CA and EG mixture under constant stirring condition. The amounts of doped Sm^{3+} are 0.5–1.5 mol%. The molar ratios of CA/Ti and CA/EG were kept constant at 2:1 and 1:1, respectively. After adjusting the pH value with ammonia to 6–7, the mixture solution was evaporated at 90 °C to gradually form a clear precursor gel. The precursor gel was baked at 150 °C in muffle furnace and expanded, then was auto-ignited at about 250 °C. The puffy, porous gray powders as-combusted was calcined at the temperature of 500–800 °C for 2 h in air.

2.2. Characterization

The crystalline structure of the samples was determined by a D/max-γA diffractometer (Cu Kα radiation, $\lambda = 0.154056$ nm) studies. The averaged grain sizes D were determined from the XRD pattern according to the Scherrer equation $D = k\lambda/\beta\cos\theta$, where k is a constant (shape factor, about 0.9), λ the X-ray wavelength (0.15418 nm), β the full width at half maximum (FWHM) of the diffraction line, and θ is the diffraction angle. The values of β and θ of anatase and rutile are taken from anatase (1 0 1) and rutile (1 1 0) diffraction line, respectively. The amount of rutile in the samples were calculated using the following equation [13]: $X_R = (1 + 0.8I_A/I_R)^{-1}$,where X_R is the mass fraction of rutile in the samples, I_A and I_R are the X-ray integrated intensities of (101) reflection of the anatase and (110) reflection of rutile, respectively. The morphology of the sample was observed using Tecnai G^2-20 transmission electron microscopy (TEM, $E_v = 200$ kV). To study the light absorption of the photocatalyst sample, the diffuse reflectance spectra (DRS) of the photocatalyst sample in the wavelength range of 200–800 nm were obtained using a UV–vis scanning spectrophotometer (Shimadzu UV-3101), while $BaSO_4$ was as a reference. The photoluminescence (PL) spectra of the samples were recorded with a Fluorescence Spectrophotometer F-4500.

2.3. Photocatalytic activity

In order to evaluate photocatalytic activity of the prepared samples, photocatalytic degradation of methylene blue (MB) was performed. For a typical photocatalytic experiment, 200 mg of the prepared TiO_2 nanocrystalline was added to 200 mL of the 100 ppm methylene blue (MB) aqueous solution. The prepared TiO_2 nanocrystalline was dispersed under ultrasonic vibration for 10 min. After keeping at least 20 min, MB concentration in the solution was found to be constant on all samples prepared. Therefore, the solution in which the prepared TiO_2 nanocrystalline was dispersed was kept in the dark for 30 min and then UV irradiation of the solution was started. For UV irradiation, a 160 W high-pressure mercury lamp (GYZ-160) fixed at a distance of 150 mm above the surface solution was used as UV light source. After recovering the catalyst by centrifugation, the light absorption of the clear solution was measured at 660 nm (λ_{max} for MB) at a set time. The decolorization of methylene blue was calculated by formula: decolorization $= (C_0 - C)/C_0$, C_0 and C is the concentration of primal and photodecomposed MB. The absorbance of the MB solution was measured was measured with a UV–vis spectrophotometer (Shimadzu UV-3101).

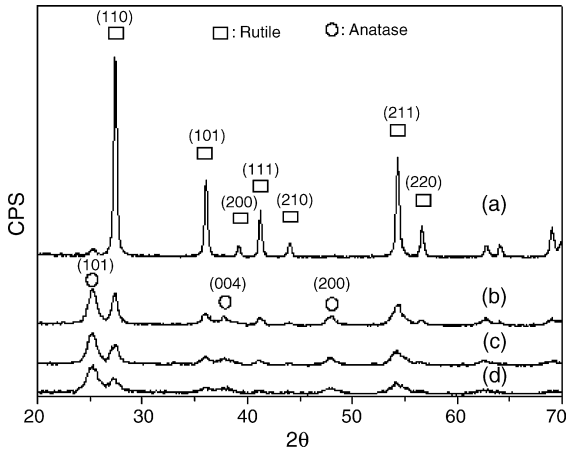

Fig. 1. XRD patterns of TiO_2 with various amounts of samarium calcined at 600 °C for 2 h. (a) Undoped, (b) 0.5 mol% Sm, (c) 1.0 mol% Sm, and (d) 1.5 mol% Sm.

3. Results and discussion

XRD patterns of Sm^{3+} ions doped titania samples with various samarium content calcined at 600 °C for 2 h are shown in Fig. 1. From these XRD results, it is shown that the X-ray diffraction peak at 25.5° corresponds to characteristic peak of crystal plane (1 0 1) of anatase, and the peak at 27.6° corresponds to characteristic peak of crystal plane (1 1 0) of rutile. In undoped titania sample calcined at 600 °C for 2 h, rutile is the dominant crystallized phase, and the sample contains 97.5% of rutile phase, while Sm^{3+}-doped TiO_2 samples shows a mixture phase of anatase and rutile, and the relative ratio of rutile to anatase is reduced with the increase of samarium content, showing that the anatase-to-rutile phase transformation was greatly inhibited by samarium ion doping. Lin et al. [14,15] also found that other rare earth ions (La, Y, and Ce) could inhibit the anatase-to-rutile phase transformation during the thermal treatment. The inhibition of the phase transition was ascribed to the stabilization of the anatase phase by the surrounding rare earth ions through the formation of Ti–O rare-earth element bonds [16]. In the present system, I think that the likely formation of Sm–O–Ti interac-

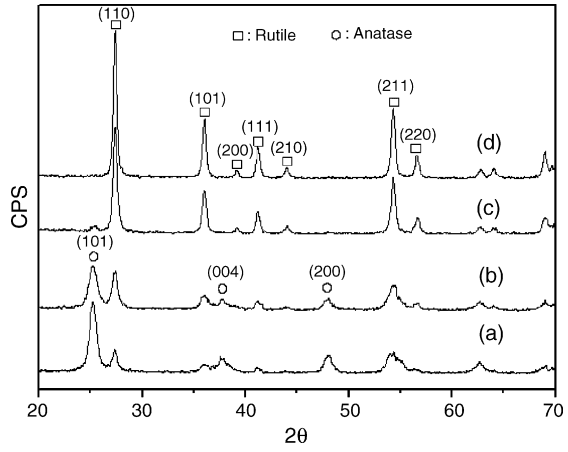

Fig. 2. XRD patterns of 0.5 mol% Sm^{3+}-doped TiO_2 calcined at different temperatures. (a) 500 °C, (b) 600 °C, (c) 700 °C, and (d) 800 °C.

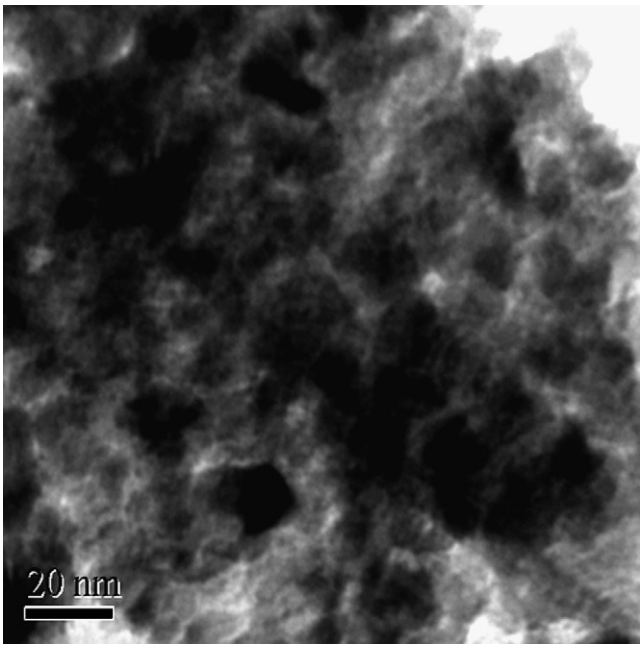

Fig. 3. TEM micrograph of 0.5% Sm^{3+}-doped TiO_2 nanocrystalline.

tion took place and inhibit the transition of the anatase phase. But the mechanism dominating in the anatase-to-rutile phase transformation process is complex and not fully understood yet. Therefore, the more detailed study should be done in the future in order to extensively understand the effect of samarium ion doping on the anatase-to-rutile phase transformation.

Fig. 2 shows the XRD patterns of TiO_2 powders doped with 0.5 mol% samarium calcined at various temperatures between 500 and 800 °C. It can be seen that no peaks from samarium oxide were observed. It was shown that the intensities of the anatase peaks decreased, while the intensities of the rutile peaks greatly increased and contents of rutile phase increased as the calcinations temperature was raised (shown in Table 1). When calcined at 800 °C, the pattern exhibits a complete rutile TiO_2 structure and it means that the phase transformation from anatase to rutile has completed at this temperature.

Fig. 3 shows a TEM image of TiO_2 nanoparticles doped with 0.5 mol% samarium calcined at 600 °C. The nanoparticles have a spherical morphology with an average diameter of 15 nm, which is in good agreement with the XRD evaluation (shown in Table 1).

To investigate the optical absorption properties of catalysts, we examined the diffuse reflectance spectra (DRS) of TiO_2 and Sm^{3+}-doped TiO_2 in the range of 220–850 nm and our results are

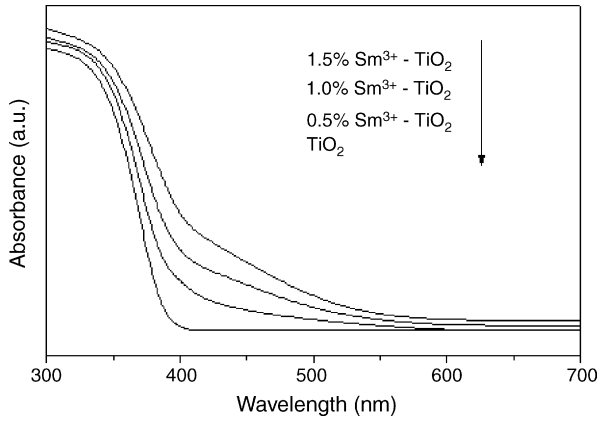

Fig. 4. UV–vis absorption spectra of pure and doped TiO_2 calcined at 600 °C for 2 h.

shown in Fig. 4. It can be seen that while TiO_2 had no absorption in the visible region (>400 nm), Sm^{3+}-doped TiO_2 had significant absorption between 400 and 500 nm, which increased with the increase of samarium ion content. In addition, it can be noted that the optical absorption in the UV region was also enhanced. Li et al. [17] reported that the band gap of TiO_2 nanoparticles was reduced by Nd^{3+} doping and the band gap narrowing was primarily attributed to the substitution Nd^{3+} ions which introduced electron states into the band gap of TiO_2 to form the new lowest unoccupied molecular orbital. In order to understand the reason of the band gap narrowing for Sm^{3+}-doped TiO_2, density functional theory calculations were in going.

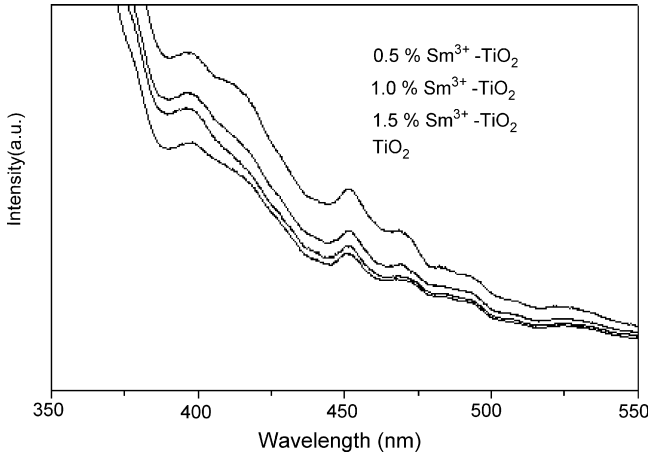

Fig. 5. PL spectrum of samarium doped TiO_2 calcined at 600 °C for 2 h with the excitation wavelength of 300 nm.

Table 1
The characteristics of Sm^{3+}-doped samples containing different samarium content calcined at 600 °C

Samarium content (%)	Anatase		Rutile		Decolourization of MB at 120 min (%)
	Crystal size $D_{(1\,0\,1)}$ (nm)	X_A (%)	Crystal size $D_{(1\,1\,0)}$ (nm)	X_R (%)	
0	–	2.41	18.8	97.59	65.3
0.5	13.8	48.39	13.6	51.61	95.6
1.0	12.9	58.22	13.1	41.78	88.8
1.5	12.5	58.33	12.8	41.67	73.9

Fig. 5 shows the PL spectrum of TiO_2 with various amounts of samarium at 600 °C for 2 h with the excitation wavelength of 300 nm. It can be seen that the undoped and doped TiO_2 nanoparticles can exhibit obvious PL signals with similar curve shape, demonstrating that samarium dopant does not give rise to new PL phenomena. TiO_2 nanoparticles could exhibit strong and wide PL signals at the range from 400 to 500 nm with the excited wavelength of 300 nm, and had two obvious PL peaks at about 400 and 450 nm, respectively, possibly the former mainly resulting from band edge free excitons, the latter mainly resulting from binding excitons [18,19]. There were lots of oxygen vacancies on the surface of TiO_2 nanoparticles, and the size of particle was fine so that the average distance the electrons could move freely was very short. These factors could make the oxygen vacancies very easily bind electrons to form excitons. Thus, the exciton energy level near the bottom of the conduction band could come into being, and the PL band of the excitons could also occur. Thus, the stronger the PL intensity, the higher the content of surface oxygen vacancy and defect. In addition, the PL intensity gradually increased as samarium content increased, and arrived at the highest degree when samarium content was 0.5 mol%. If samarium contents continued to increase, namely more than 0.5 mol%, the PL intensity began to go down. These results demonstrated that the content of surface oxygen vacancy arrived at the highest degree when samarium content was 0.5 mol%.

The photocatalytic degradation of methylene blue (MB) over Sm^{3+}-doped TiO_2 samples calcined at 600 °C by LCS method is evaluated and the results are shown in Fig. 6. It is obvious from Fig. 6 that all Sm^{3+}-doped TiO_2 samples with various samarium ion concentrations (from 0.5 to 1.5 mol%) exhibit higher photoactivities than that of undoped TiO_2, and 0.5 mol% Sm^{3+}-doped TiO_2 shows the highest photocatalytic activity, which suggests that the Sm^{3+} doping enhances the photocatalytic activity of TiO_2 and there is an optimum doping content of Sm^{3+} ions in TiO_2 particles. From Table 1, it can be seen that samarium doping content has little influence on grain size and rutile content of all the samples. Xu et al. [20] reported that there exists an optimum doping content of rare earth ions in TiO_2 particles for the most efficient separation of photoinduced electron–hole pairs. According to Figs. 5 and 6, it can be found that the order of photocatalytic activity was the same as that of PL intensity,

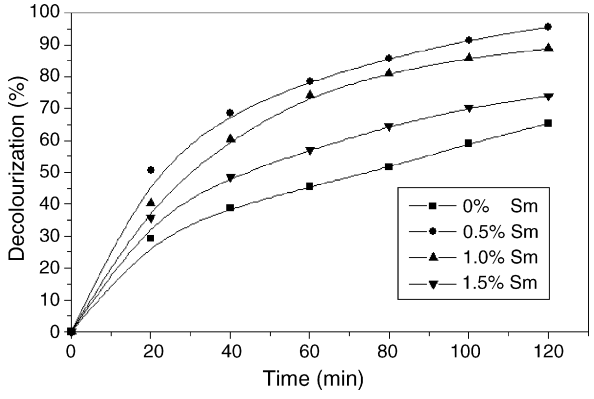

Fig. 6. Photocatalytic decomposition profiles of methylene blue. Over different samarium doped TiO_2 nanoparticle calcined at 600 °C for 2 h.

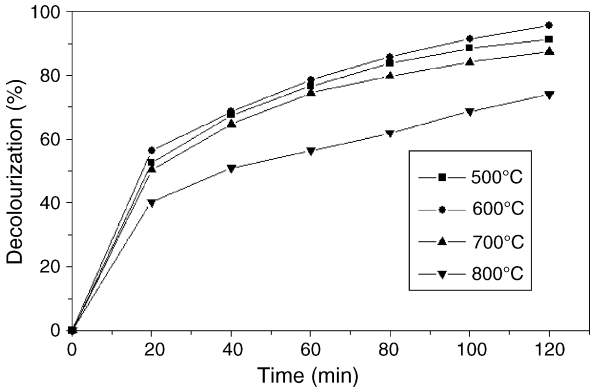

Fig. 7. Photocatalytic decomposition profiles of methylene blue. Over 0.5 mol% Sm^{3+}-doped TiO_2 nanocrystalline calcined at different temperatures.

namely, the stronger the PL intensity, the higher the photocatalytic activity. During the process of PL, oxygen vacancies and defects could bind photoinduced electrons to form free or binding exactions so that PL signal could easily occur, and the larger the content of oxygen vacancies or defects, the stronger the PL intensity. But, during the process of photocatalytic reactions, oxygen vacancies and defects could become the centers to capture photoinduced electrons so that the recombination of photoinduced electrons and holes could be effectively inhibited. Moreover, oxygen vacancies could promote the adsorption of O_2, and there was strong interaction between the photoinduced electrons bound by oxygen vacancies and adsorbed O_2. This indicated that the binding for photoinduced electrons of oxygen vacancies could make for the capture for photoinduced electrons of adsorbed O_2, and O_2 free group was produced at the same time. Thus, oxygen vacancies and defects were in favor of photocatalytic reactions in that O_2 was active to promote the oxidation of organic substances [21,22]. The above results demonstrated that there were certain relationships between PL spectra and photocatalytic activity, namely, the stronger the PL intensity, the larger the content of oxygen vacancies and defects, the higher the photocatalytic activity. Therefore, in this study 0.5 mol% may be the most suitable content of Sm^{3+} in the titania, at which the recombination of photoinduced electrons and holes could be effectively inhibited and thereby the highest photocatalytic activity is formed.

Fig. 7 shows the results of photocatalytic degradation of methylene blue (MB) over TiO_2 doped with 0.5 mol% samarium, which were prepared at various calcinations temperatures. It is found that the photocatalytic activity is reduced considerably for the samples calcined at 800 °C and Sm^{3+}-doped TiO_2 calcined at 600 °C showed the highest photocatalytic activity among the all samples. From Table 2, it can be seen that calcination temperatures have the most significant effect on the rutile content, while grain size of all the samples calcinated at different temperature are nearly equal and the rutile fraction increases with increasing calcination temperature. Recently, it has been found that a mixture of anatase and rutile TiO_2 nanoparticles has a much higher photocatalytic activity than pure anatase or pure rutile TiO_2 nanoparticles [23]. The remarkable coexistent effect of rutile and anatase would arise from the increase in

Table 2
The characteristics of 0.5 mol% Sm^{3+}-doped TiO_2 calcined at different temperatures

Calcinations temperature (°C)	Anatase		Rutile		Decolourization of MB at 120 min (%)
	Crystal size $D_{(1\,0\,1)}$ (nm)	X_A (%)	Crystal size $D_{(1\,1\,0)}$ (nm)	X_R (%)	
500	13.1	74.7	12.8	25.3	91.3
600	13.8	48.39	13.6	51.61	95.6
700	–	5.9	14.7	94.1	87.4
800	–	0	16.3	100	74

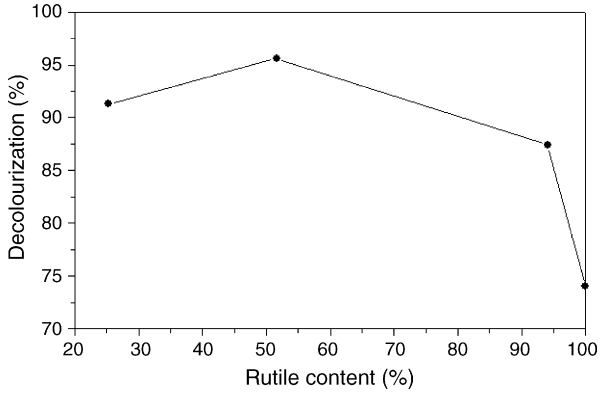

Fig. 8. Photocatalytic deodorization of methylene blue. Over 0.5 mol% Sm^{3+}-doped TiO_2 nanocrystalline containing different rutile content.

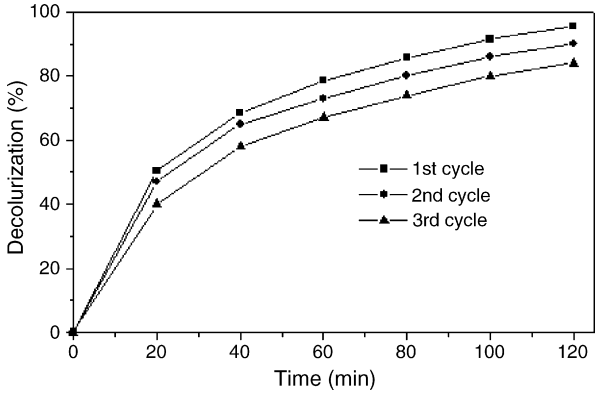

Fig. 9. Deactivation profiles of 0.5 mol% Sm^{3+}-doped TiO_2 nanocrystalline calcined at 600 °C for 2 h.

the charge separation efficiency due to photo-induced interfacial electron transfer from anatase to rutile [24]. But until now, there were no reports about synergistic effect between anatase and rutile for doped TiO_2 samples. In order to investigate the role of rutile content in photcatlytic activity for our Sm^{3+}-doped TiO_2 nanocrystalline, Fig. 8 shows the relation of the rutile content to the phtocatalytic activity of anatase and rutile TiO_2 mixture. It is clear that the photocatalytic activity of is drastically increased under the presence of a small amount of anatase phase (only 5.9% anatase) compared to pure rutile and the sample calcined at 600 °C consists of mixed phases with 51.61% rutile shows the highest photocatalytic activity. These results strongly suggest the existence of a synergistic effect between anatase and rutile powders in the Sm^{3+}-doped TiO_2, which is siminar to that of undoped TiO_2 [23,24].

In addition, deactivation over 0.5 mol% Sm^{3+}-doped TiO_2 samples calcined at 600 °C by LCS method has been further studied. Once the degradation of MB was complete, the reaction was stopped and the second cycle was started after making the initial concentration of MB to 100 ppm. Similarly, the third cycle was also carried out. Here, the catalyst is taken at the end of the first cycle and used for the second cycle and the catalyst at the end of the second cycle is used for the third cycle. The degradation profiles of first, second and third cycle over 0.5 mol% Sm^{3+}-doped TiO_2 samples calcined at 600 °C by LCS method is shown in Fig. 9. It can be seen that the efficiency has not decreased even for the third cycle, which can still decolorize 85% of methylene blue in 120 min. Nagaveni et al. [25] also reported that combustion synthesized TiO_2 was not easier to undergo deactivation compared with Degussa P-25.

Above all, photocatalytic degradation experiments indicated that doping samarium ions in TiO_2 could enhance photocatalytic activity in photocatalytic decomposition of methylene blue. The increase in activity is probably due to prevention of electron–hole recombination, lower band gap by samarium doping and the existence of a synergistic effect between anatase and rutile.

4. Conclusion

High photocatalytic activity of Sm^{3+}-doped TiO_2 nanocrystalline has been successfully prepared by low temperature combustion synthesis (LCS). The samarium doping was found to significantly inhibit the anatase-to-rutile phase transformation. The highest enhancement in photoreactivity was obtained at 0.5 mol% samarium ions doping, which may be in favor of the most efficient separation of the charge carriers. The results of photocatalytic degradation of methylene blue (MB) over 0.5 mol% Sm^{3+}-TiO_2 prepared at various calcination temperatures show that the photocatalytic activity is drastically increased under the presence of a small amount of anatase phase (only 5.9% anatase) compared to pure rutile, and the sample calcined at 600 °C consists of mixed phases with 51.61% rutile shows the highest photocatalytic activity, which suggests the existence of a synergistic effect between anatase and rutile powders.

Acknowledgements

This work was supported by the Provincial Excellent Ph.D. Thesis Research Program of Hunan (no. 2004-141) and the

Postgraduate Educational Innovation Engineering of Central South University (no. 2005-22).

References

[1] M.R. Hoffmann, S.T. Choi, W. Martin, D.W. Bahnemann, Chem. Rev. 95 (1995) 69–96.
[2] A. Fujishima, T.N. Rao, D.A. Truk, J. Photochem. Photobiol. C: Photochem. Rev. 1 (2000) 1–21.
[3] W. Choi, A. Termin, M.R. Hoffmann, J. Phys. Chem. 98 (1994) 13669–13679.
[4] D.H. Kim, S.I. Woo, et al., Solid State Commun. 136 (2005) 554–558.
[5] Akihiko Hattori, Yoshifumi Tokihisa, et al., J. Electrochem. Soc. 147 (2000) 2279–2283.
[6] Cun Wang, Bo-Qing Xu, J. Solid State Chem. 178 (2005) 3500–3506.
[7] V. Iliev, D. Tomova, et al., Appl. Catal. B: Environ. 63 (2006) 266–271.
[8] K.T. Ranjit, I. Willner, et al., J. Catal. 204 (2001) 305–313.
[9] Yuhong Zhang, Hailiang Xu, et al., J. Photochem. Photobiol. A: Chem. 170 (2005) 279–285.
[10] Yan Xiaoli, Jing He, et al., Appl. Catal. B: Environ. 55 (2005) 243–252.
[11] Yibing Xie, Chunwei Yuan, et al., Mater. Sci. Eng. B 117 (2005) 325–333.
[12] Chyi-Ching Hwang, Tsung-Yung, et al., Mater. Sci. Eng. B 111 (2004) 49–56.
[13] R.A. Spurr, H. Myers, Anal. Chem. 29 (1957) 760–762.
[14] J. Lin, J.C. Yu, D. Lo, S.K. Lam, J. Catal. 183 (1999) 368–372.
[15] J. Lin, J.C. Yu, J. Photochem. Photobiol. A: Chem. 116 (1998) 63–67.
[16] E.L. Crepaldi, G.J. de, A.A. Soler-Illia, D. Grosso, F. Cagnol, F. Ribot, C. Sanchez, J. Am. Chem. Soc. 125 (2003) 9770–9786.
[17] W. Li, Y. Wang, H. Lin, S. Ismat Shah, C.P. Huang, D.J. Doren, S.A. Rykov, J.G. Chen, M.A. Barteau, Appl. Phys. Lett. 83 (2003) 4143–4145.
[18] L.D. Zhang, C.M. Mo, Nanostruct. Mater. 6 (1995) 831–834.
[19] Danzhen Li, Yi Zheng, Xianzhi Fu, Chin. J. Mater. Res. 14 (2000) 639–644.
[20] A.-W. Xu, Y. Gao, H.-Q. Liu, J. Catal. 207 (2002) 151–157.
[21] A.L. Linsebigler, G. Lu, J.T. Yates, Chem. Rev. 95 (1995) 735.
[22] H. Liu, S. Cheng, M. Wu, H. Wu, J. Zhang, W. Li, C. Cao, J. Phys. Chem. A 104 (2000) 7016.
[23] D.C. Hurum, A.G. Agrios, K.A. Gray, T. Rajh, M.C. Thurnauer, J. Phys. Chem. B 107 (2003) 4545–4549.
[24] Takahira Miyagi, Masayuki Kamei, et al., Chem. Phys. Lett. 390 (2004) 399–402.
[25] K. Nagaveni, G. Sivalingam, M.S. Hegde, G. Madras, Appl. Catal. B: Environ. 48 (2004) 83–93.